Canadian Conference - Pacific Conference on Earthquake Engineering 2023

Vancouver, British Columbia

June 25th – June 30th, 2023

Accuracy and Uncertainty of Predicted Maximum and Residual Displacements of RC Bridge Columns Under Earthquake Excitations

Saif Aldabagh[1*], Faroque Hossain[2] and George M. Shahria Alam [3]

[1]Bridge Engineer, COWI North America, North Vancouver, BC, Canada
[2]PhD Student, Applied Laboratory for Advanced Materials & Structures (ALAMS), School of Engineering, The University of British Columbia, Kelowna, BC, Canada
[3]Professor and Tier-1 Principal's Research Chair in Resilient & Green Infrastructure, School of Engineering, The University of British Columbia, Kelowna, BC, Canada
[*]saif.aldabagh@ubc,ca (Corresponding Author)

ABSTRACT

Fundamental to the performance-based seismic design is the accuracy of predicted responses under earthquake excitations. This study evaluates the accuracy and uncertainty of predicted maximum and residual displacements of concrete bridge columns subjected to different types of ground motions. A series of nonlinear time-history analyses considering a wide range of element formulations and model parameter combinations was performed to reproduce measured responses from previous shake table tests. Variations in element formulation had little influence on the accuracy and uncertainty of predicted maximum displacements. The gradient inelastic force-based element, however, predicted bar tensile strain profiles across the plastic hinge with higher resolution, but at a higher computational cost than displacement-based and beam with hinges elements. Models with tangent stiffness-based Rayleigh damping produced the most accurate predictions of the maximum drift ratios with an RMSE of 0.011, indicating that the maximum displacement (or drift ratio) can be predicted with reasonable accuracy. Residual displacements, on the other hand, were predicted with unreasonable levels of error and uncertainty. A data-driven model was thus proposed to correct predicted residual displacement.

INTRODUCTION

In seismic performance assessments, beam-column members have been generally modeled using either concentrated (or lumped) plasticity or distributed plasticity elements. The latter are superior to the former primarily because they allow the plastic hinge to form at any location and account for axial-flexural interactions, and thus are the focus of this study. Several recent studies have quantified the accuracy of the predicted seismic responses of bridge columns and their sensitivity to various modeling assumptions. However, in the vast majority of these studies, experimental data used were for concrete bridge columns tested under quasi-static cyclic tests, which do not reproduce realistic earthquake conditions ([1-6], among others). Because of this limitation, the ability of various modeling formulations to predict a key response parameter characterizing the post-earthquake condition of bridges, the residual displacement, may not be assessed. Similar studies but considering experimental data from shake table tests on concrete bridge columns exist though are limited.

Hachem et al. [7] undertook one of the early research efforts to evaluate the accuracy of different modeling approaches in predicting the dynamic responses of concrete bridge columns to earthquake loading. They compared results predicted using flexibility-based fiber elements with different discretization schemes to experimental data from their shake table tests. The accuracy of the predicted local deformations was found to be highly sensitive to the number of integration points [7]. Similarly, based on results from their shake table tests, Sakai et al. [8] reported that varying the damping assumptions improved the predictions of the maximum drift but not the residual drift. Berry and Eberhard [9] adopted a modified concrete model [10] accounting for the imperfect crack closure to predict the dynamic response of a bridge column. Variations in this model were found to improve the predictions of residual displacements, particularly for distributed plasticity elements. Similar improvements to the predicted residual displacements were reported by Lee and Billington [11] and Moshref et al. [12] while using the same concrete model. Reproduced responses by Yazgan and Dazio [13, 14] for RC specimens under shake table excitation showed that the accuracy of the predicted residual displacements is much lower than the maximum displacements irrespective of the modeling strategy. In a similar study by Sousa et al. [15], despite the variation in the modeling assumptions, an acceptable level of accuracy in residual estimates was not achieved. They emphasized the need for a future study considering a wider set of experimental shake table tests to consolidate the findings of the previous studies and to propose a refined approach to predict post-earthquake residual displacements. More recently, Akbari and Khanmohammadi [16] carried out a comprehensive parametric investigation assessing the accuracy of predicted dynamic responses for bridge columns under near-field motions. They also proposed two methods to improve the predictions of residual displacements. The superior method is considered in this study for comparison purposes and is briefly described in a later section.

While the above-described studies have provided a wealth of information on the analytical prediction of the dynamic responses, and the residual displacement, in particular, they were, as evident, either specific to a certain type of ground motion or considered a narrow set of shake table test data. Because of this, a general procedure to refine the predicted residual displacement responses remains absent from the literature. The overarching objective of this study is to propose a new method to improve the accuracy of the predicted residual displacements. Contrary to the previous methods, the proposed method is applicable to bridge columns with a wide range of material properties, geometry, and reinforcement details; and under different types of ground motions. To achieve the objective of this study, a comprehensive parametric investigation is first executed to evaluate the accuracy and uncertainty of estimates of the maximum and residual displacements for concrete bridge columns. This study also employs results from eleven shake table tests making it the first to consider such a wide set of experimental data for concrete bridge columns. State-of-the-art machine learning-based symbolic regression is implemented in this study to fit the predicted residual displacement data into a correction model.

MODELING STRATEGIES

The first modeling strategy is based on a plastic hinge integration method where the locations and weights of element integration points (IPs) are adjusted such that the weight of end IPs is equal to the plastic hinge length. In this method, two-point Gauss integration is used for the element interior while two-point Gauss-Radau integration is applied over a length of $4L_p$ at each end of the element, where L_p is the plastic hinge length, resulting in a six-IP element. This element is available in OpenSees [17] and is known as *beamWithHinges* (BwH). The resolution of the predicted strain/curvature field over the member length, however, cannot be increased when using the BwH element because of the fixed number of IPs. Another limitation of the BwH element is that, for elements with equal plastic hinges at both ends, the weights of two interior integration points become negative when the length of the element is less than $8L_p$ which is common for concrete bridge columns.

In the second modeling strategy, the plastic hinge region is modeled using a single displacement-based (DB) element with two IPs. In a displacement-based formulation, localization occurs due to strain concentration in elements subjected to the highest bending moment. In a discretized cantilever concrete bridge column, for example, the element closest to the base is, therefore, the most susceptible to localization. Taking the length of this element as L_p forces localization within the plastic hinge region and thus maintains response objectivity. This, however, results in linear curvature distribution over the plastic hinge region which is not realistic, particularly for inelastic responses. Despite this shortcoming, this method has been found to accurately predict global as well as local responses at critical sections (i.e., sections of the maximum moment) of concrete bridge columns under cyclic loading [18, 19].

The third modeling strategy employs the gradient inelastic force-based (GI FB) element which has been recently introduced into OpenSees and is known as *gradientInelasticBeamColumn.* The element is based on the gradient inelastic beam theory which has been formulated by Sideris and Salehi [20] primarily with the intent of eliminating strain singularities prevalent in the classical beam theory. In this formulation, a set of gradient nonlocality relations associating the material section strains of the constitutive relations with the macroscopic section strains of the strain–displacement equations are introduced. These relations include a Heaviside function that modifies their form at locations experiencing strain softening to ensure the boundedness of the material section strain fields and response objectivity. The superiority of the GI FB over the previous two formulations in terms of the accuracy of predicted responses, particularly curvature and strain distributions across element length, is demonstrated by Salehi et al. [5] through comparisons with experimental data.

MODEL PARAMETERS

NTHA in this study was performed using a fiber-based analysis software, OpenSees [17]. Combinations of model parameters considered in this study are listed in Table 1. Combination 1 served as the control combination. Details of the selected models and their variable parameters are provided next.

Concrete material models

Three different constitutive relationships were used in this study to model the cyclic behavior of concrete. These are OpenSees *Concrete01*, *Concrete04*, and *Concrete01WithSITC* (hereafter referred to as SITC). While both models use the same loading and unloading rules by Karsan and Jirsa [21], the cyclic response envelope of Concrete01 is based on Kent-Scott-Park concrete model [22], whereas that of Concrete04 is based on Popovics concrete model [23]. Concrete01 assumes that the concrete maintains its compressive strength following the crushing of concrete and ignores the contribution of the tensile strength of concrete. On the contrary, Concrete04 assumes that the compressive strength rapidly degrades to zero at the concrete crushing, and accounts for the contribution of the tensile strength of concrete. In Concrete 04, the monotonic tensile envelope of concrete is assumed to have a linear stress-strain relationship up to the tensile strength followed by an exponential decay up to the ultimate tensile strain of concrete. SITC, on the other hand, is identical to Concrete01 but accounts for the effect of imperfect crack closure. Imperfect crack closure is a phenomenon typically observed in concrete elements under cyclic loading where tension cracks become partially filled with small particles of concrete sediments, causing load transfer before cracks completely close. Stanton and McNiven [24] proposed a modification to the loading and unloading rules of Karsan and Jirsa [21] where an alternative load path is activated if the reloading strain (ε_r) is exceeded. In the alternative load path, the concrete reloads at ε_r rather than the previous unloading strain under cyclic loading. ε_r has a physical correlation with crack width since at ε_r cracks are assumed to open to a level where they can trap particles. The properties of the confined concrete in this study were determined based on the theoretical stress-strain model proposed by Mander et al. [25] for confined concrete.

Reinforcing steel material models

Reinforcing steel materials models considered in this study are OpenSees *Steel01*, *Steel02*, *Dodd-Restrepo*, and *ReinforcingSteel*. Steel01 idealizes the envelope of the stress-strain hysteresis as an elastoplastic bilinear relation making it the simplest among the four models. In this relation, the post-yield tangent is taken as a fraction of the initial elastic tangent to account for strain hardening. Steel02, which is the most common, is based on the Giuffre-Menegotto-Pinto constitutive relation [26]. It captures the Bauschinger effect and the cyclic isotropic hardening. Dodd-Restrepo was developed by Dodd and Restrepo [27] to capture additional characteristics of the cyclic stress-strain response of steel. These include the reduction of the unloading modulus with the plastic strain and the correlation between the maximum compressive strain and the reduction in the ultimate tensile strain. ReinforcingSteel was developed by Kunnath et al. [28] and is largely based on Chang and Mander [29]'s model. A unique feature of the ReinforcingSteel is its ability to capture the diminishing yield plateau under plastic strain reversals. Low-cycle fatigue damage accumulation (D_f) in steel bars can be accounted for in OpenSees through the *Fatigue* model.

Bond slip models

Reinforcement slip from adjacent anchorage zones results in additional flexibility that must be accounted for in the analysis. To this end, two widely used bond slip models are considered in this study. In the first, elastic springs with rotational stiffness are added at member ends. The second model is OpenSees *Bond_SP01* by Zhao and Sritharan [30]. In fiber-based analysis, Bond_SP01 is added to a zero-length section element at the intersection between the flexural member and an adjoining member representing a footing or joint. The section of the zero-length element is identical to that of the beam-column element except for the steel fibers which are assigned the Bond_SP01 model instead of the reinforcing steel model. Detail description of the parameters required to define the Bond_SP01 can be found in Zhao and Sritharan [30].

Damping models

A significant research effort has gone into studying the consequences of inappropriate idealization of damping in NTHA [31, 32, 33, Among others]. An issue consistently reported in these studies is that the Rayleigh damping model may generate spurious damping forces practically during regimes of inelastic response. A number of remedies have been thus proposed. Hall [31] suggested eliminating the mass-proportional damping term. This has been found to improve the accuracy of the predicted responses [34, 12]. Charney [32] and Petrini et al. [35] recommended formulating the damping matrix based on tangent stiffness instead of initial stiffness. This will reduce the damping forces when the tangent stiffness reduces during yielding and softening, hence resulting in better predictions. One implication for adopting the tangent stiffness, however, is that sudden and intense changes in stiffness can cause convergence difficulties. Also, at large deformations with the effects of gravity loads included, the structural tangent stiffness, and therefore damping, may become negative leading to inaccurate response predictions [33]. Because of such limitations and the lack of physical basis, the tangent stiffness approach was deemed inappropriate by Chopra and McKenna [33]. The damping ratio (ζ) is another parameter that plays a critical role in the formulation of the damping matrix. While remaining open for debate, ζ values ranging from 2% to 5% have been the most common for RC structures. In review of the literature and as evident from the above brief discussion on damping, it appears that findings from studies on damping models do not converge to a single universally acceptable formulation. As a result, this study considers four different strategies to formulate the Rayleigh damping matrix. These are K-proportional damping with initial stiffness matrix and ζ of 2%; K-M proportional damping with initial stiffness matrix and ζ of 2%; K- proportional damping with initial stiffness matrix and ζ of 2%; K- proportional damping with initial stiffness matrix and ζ of 2%. In shake table tests considered in this study, changes in damping ratios across the frequency range were found to be insignificant and diminish as damage progresses. Hence, in the analysis, ζ held a constant value within the frequency range.

Strain rate effect

Under dynamic loads, material properties may be affected by the strain rate. The strain rate effect on the properties of concrete and reinforcing steel bars is typically accounted for in analysis through dynamic amplification factors. Mander et al. [25] proposed dynamic amplification factors correlating the quasi-static compressive strength, modulus of elasticity, and strain at peak stress of concrete with the strain rate ($\dot{\varepsilon}$). Malvar and Crawford [36] proposed similar factors but to adjust the yield and ultimate stresses of reinforcing steel bars due to changes in strain rate. These factors are considered in this study to account for the strain rate effect. Strain rates characteristic of seismic response typically range from 0.01 to 0.10 S^{-1} [37]. The $\dot{\varepsilon}$ is therefore treated as a variable in this study with values equal to 0 (i.e., no strain rate effect), 0.01, 0.05, and 0.1 to evaluate the effect of strain rate on the accuracy and uncertainty of predicted responses.

Table 1. Combinations of model parameters.

Comb.	Concrete model	Steel model	Bond Slip model	Damping model	Stiffness matrix	Damping ratio (%)	Strain rate (s^{-1})
1	Concrete04	Steel02	Bond_SP01	K proportional	Initial	2	0
2	Concrete01	Steel02	Bond_SP01	K proportional	Initial	2	0
3	Concrete01WithSITC (ε_r=0.01)	Steel02	Bond_SP01	K proportional	Initial	2	0
4	Concrete01WithSITC (ε_r=0.02)	Steel02	Bond_SP01	K proportional	Initial	2	0
5	Concrete01WithSITC (ε_r=0.03)	Steel02	Bond_SP01	K proportional	Initial	2	0
6	Concrete04	ReinforcingSteel	Bond_SP01	K proportional	Initial	2	0
7	Concrete04	Dodd-Restrepo	Bond SP01	K proportional	Initial	2	0
8	Concrete04	Steel01	Bond SP01	K proportional	Initial	2	0
9	Concrete04	Steel02	Bond_SP01 (R_c=0.7)	K proportional	Initial	2	0
10	Concrete04	Steel02	Bond_SP01 (R_c=0.9)	K proportional	Initial	2	0
11	Concrete04	Steel02	Elastic Spring	K proportional	Initial	2	0
12	Concrete04	Steel02	Bond_SP01	K-M Proportional	Initial	2	0
13	Concrete04	Steel02	Bond_SP01	K proportional	Tangent	2	0
14	Concrete04	Steel02	Bond_SP01	K proportional	Initial	5	0
15	Concrete04	Steel02	Bond_SP01	K proportional	Initial	2	0.01
16	Concrete04	Steel02	Bond_SP01	K proportional	Initial	2	0.05
17	Concrete04	Steel02	Bond_SP01	K proportional	Initial	2	0.1

SELECTED SHAKE TABLE TEST DATA

To evaluate the levels of accuracy and uncertainty associated with simulated responses, a set of RC bridge columns tested under shake table excitations is considered. Key properties of these columns as well as their input motions are provided in Table 2. All of the selected specimens were circular in cross-section with single curvature and flexure dominant response and were subjected to unidirectional excitations. A total of 82 earthquake simulation tests were conducted on the selected specimens. This provided a wealth of experimental data to benchmark predicted responses in this study. The selected specimens were subjected to different types of ground motions. Specimens NF1, NF2, MN, and ETN were subjected to near-fault pulse motions. Specimens LD-J1, LD-J2, and LD-C1 were subjected to long-duration ground motions. Ordinary ground motions (i.e., with no special attributes) were applied to the remaining specimens. In this study, for most of the specimens, the table acceleration feedback is used in the analysis to minimize error related to the differences between target and achieved accelerations. The selected specimens were generally subjected to ground motions with incrementally increasing intensities to generate a wide range of responses from elasticity to yielding and finally to collapse. In shake table tests, safety systems in the form of cables and steel frames are typically utilized to control deformations under strong ground motions. Experimental results from simulations where such safety systems were engaged were excluded in this study as they may contribute to the prediction error and uncertainty. Further details on the experimental setup and instrumentation of the specimens can be found in relevant publications.

NUMERICAL MODEL DESCRIPTION

A representative idealization of the selected specimens is shown in Fig. 1. The columns were represented by beam-column elements whose formulation and discretization were based on the previously described three modeling strategies. Mass blocks representing the superstructure in the shake table tests were simulated in this study using lumped mass, m, as shown in Fig. 1. A rigid link was used to connect the top of the column to the center of gravity of the mass blocks. Depending on the adopted bond slip model, either a zero-length section element or rotational spring was used at the interface between the beam-column element and the fixed support. The column section was discretized into reinforcing steel, unconfined concrete, and confined concrete fibers, which were defined using the selected constitutive material models described earlier.

Table 2. Details of selected specimens and their input motions.

Exp. Program	Spec. ID	L (mm)	D (mm)	f_c' (MPa)	f_y (MPa)	f_{yh} (MPa)	ρ_l (%)	ρ_s (%)	P/P_o
Laplace [38]	9F1	1829	406	37.4	448	397	2.0	1.00	0.10
	9F2	1829	406	38.1	448	397	2.0	1.00	0.10
Phan [39]	NF1	1829	406	41.3	469	396	2.0	0.92	0.08
	NF2	1829	406	42.4	469	396	2.2	1.10	0.08
Choi [40]	MN	1600	356	43.8	486	428	2.9	1.37	0.06
	ETN	2756	356	44.0	486	428	2.9	1.54	0.06
Schoettler et al. [41]	PEER	7320	1220	42.0	519	338	1.6	0.95	0.05
Mohammed [42]	LD-J1	1829	406	37.2	510	621	2.2	1.10	0.08
	SD-L	1829	406	39.3	510	621	2.2	1.10	0.08
	LD-C1	1829	406	40.7	510	621	2.2	1.10	0.08
	LD-J2	1829	406	41.7	510	621	2.2	1.10	0.08

Exp. = experimental; Spec. = specimen; L = column length; D = column diameter; f_c' = concrete compressive strength; f_y = longitudinal reinforcement yield strength; f_{yh} = transverse reinforcement yield strength; ρ_l = longitudinal reinforcement ratio; ρ_s = spiral reinforcement ratio; P/P_o = axial load ratio; PGA = table peak ground acceleration; and EQ = earthquake simulation.

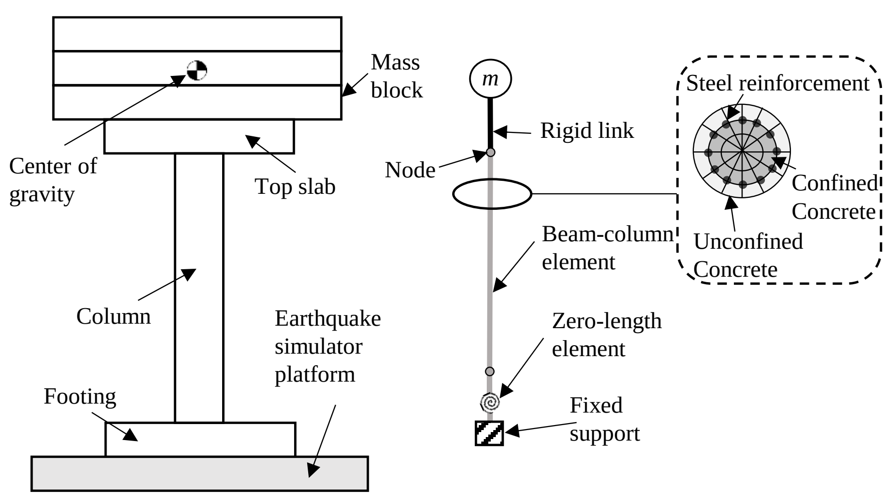

Figure 1. Model idealization of an RC bridge column tested under shake table excitations.

MAXIMUM DISPLACEMENT

Means (μ) and coefficients of variation (COV) of the ratio of predicted maximum displacement ($\Delta_{\text{max.}}^{\text{pred.}}$) to measured maximum displacement ($\Delta_{\text{max.}}^{\text{meas.}}$), as well as root-mean-square errors (RMSE) of predicted maximum drift ratios for all element formulations and model parameter combinations, are presented in Table 3. Figs 2 and 3 plot μ and COV of $\Delta_{\text{max.}}^{\text{pred.}}/\Delta_{\text{max.}}^{\text{meas.}}$ for all element formulations and model parameter combinations, respectively. Fig. 4 plots the RMSE of the predicted maximum drift ratio for all element formulations and model parameter combinations.

As seen in Table 3 and Figs. 2-4, while insignificant, varying element formulation influences the predicted maximum displacements. Predictions of models implementing the DB element were characterized by the least μ of $\Delta_{\text{max.}}^{\text{pred.}}/\Delta_{\text{max.}}^{\text{meas.}}$ maximum displacement with an average value of 0.74. This indicates that there is a higher chance of underestimating maximum displacement when using the DB element as opposed to GI FB and BwH elements. COV of $\Delta_{\text{max.}}^{\text{pred.}}/\Delta_{\text{max.}}^{\text{meas.}}$ were slightly influenced by the element formulation with average values of 0.27, 0.26, and 0.25 for DB, GI FB, BwH elements, respectively. GI FB and Bwh elements, however, are characterized by slightly higher overall accuracy than the DB element. The average RMSE of the predicted maximum drift ratio is 0.016 for both GI FB and BwH elements whereas that of the DB element is 0.02. Fig. 5 plots the measured and predicted displacement time histories and strain profiles at peak displacement for the PEER specimen under EQ3. Numerical predictions in Fig. 5 are based on the control combination, Comb 1. Measured strain profiles in Fig. 5 (b) were recorded from strain gauges installed on two longitudinal reinforcing bars at both East and West faces of the column. Predicted local responses differ with the type of element, as illustrated in Fig. 5 (b). While all predicted strain profiles were in fairly good agreement with the experimental results on both East and West faces of the column, those associated with the GI FB element had the highest resolution because of the higher number of integration points.

Variation in the concrete models and their parameters in Combinations 2-5 influenced the predicted maximum displacements. Concrete01 and SITC increased the predicted maximum displacement for the three element formulations. Using alternative reinforcing steel models had little to no effect on the predicted maximum displacements. Similar to the steel models, variations in the bond slip models and their parameters marginally influenced predicted maximum displacements, as seen in Table 3 and Figs. 2-4. On the contrary, variation in damping models and ratios noticeably influenced predicted maximum displacements for the three element formulations. Predicted maximum displacements were less underestimated with *K-M* proportional damping model (Comb. 12) than *K* proportional damping (Comb. 1), and thus were characterized by higher μ of $\Delta_{\text{max.}}^{\text{pred.}}/\Delta_{\text{max.}}^{\text{meas.}}$ and lesser RMSEs, as shown in Table 3, for the three element formulations. Accounting for the strain rate effect in Combs. 15-17 with $\dot{\varepsilon}$ ranging from 0.01 to 0.1 had a marginal influence on the μ and COV of $\Delta_{\text{max.}}^{\text{pred.}}/\Delta_{\text{max.}}^{\text{meas.}}$ and the RMSE of the predicted maximum drift ratios, as seen in Table 3 and Figs. 2-4.

Table 3. Mean (μ) and coefficient of variation (COV) of ratio of predicted ($\Delta_{pred.}$) to measured ($\Delta_{meas.}$) maximum displacement; and root-mean-square error (RMSE) of predicted maximum drift ratio for all element formulations and model parameter combinations.

Comb.	Element formulation								
	DB			GI FB			BwH		
	μ	COV	RMSE	μ	COV	RMSE	μ	COV	RMSE
1	0.71	0.26	0.021	0.81	0.27	0.016	0.78	0.24	0.016
2	0.74	0.24	0.020	0.83	0.22	0.014	0.82	0.22	0.015
3	0.74	0.22	0.019	0.80	0.22	0.016	0.82	0.22	0.014
4	0.80	0.27	0.016	0.85	0.25	0.014	0.86	0.24	0.013
5	0.83	0.29	0.016	0.91	0.30	0.015	0.93	0.28	0.014
6	0.75	0.30	0.020	0.78	0.31	0.016	0.80	0.27	0.016
7	0.72	0.28	0.021	0.69	0.31	0.018	0.81	0.30	0.018
8	0.70	0.26	0.022	0.77	0.24	0.016	0.76	0.24	0.018
9	0.71	0.26	0.021	0.81	0.26	0.015	0.78	0.24	0.016
10	0.70	0.25	0.021	0.81	0.26	0.015	0.78	0.24	0.016
11	0.75	0.23	0.022	0.84	0.20	0.016	0.82	0.19	0.017
12	0.80	0.24	0.015	0.85	0.26	0.014	0.83	0.22	0.013
13	0.97	0.26	0.011	0.99	0.26	0.011	0.98	0.25	0.011
14	0.56	0.29	0.030	0.60	0.24	0.026	0.60	0.28	0.024
15	0.68	0.29	0.023	0.77	0.29	0.017	0.75	0.27	0.017
16	0.67	0.30	0.023	0.75	0.30	0.018	0.76	0.30	0.018
17	0.66	0.31	0.023	0.73	0.30	0.018	0.74	0.31	0.018

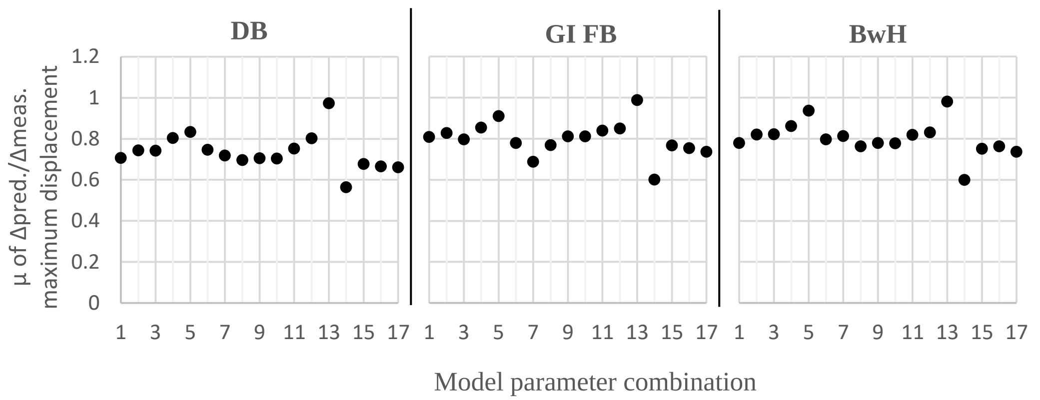

Figure 2. Mean (μ) of ratio of predicted to measured maximum displacement for all element formulations and model parameter combinations.

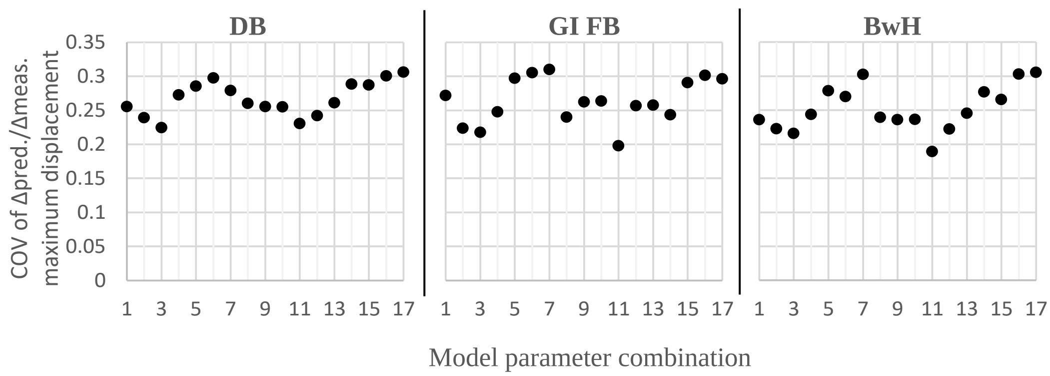

Figure 3. Coefficient of variation (COV) of ratio of predicted to measured maximum displacement for all element formulations and model parameter combinations.

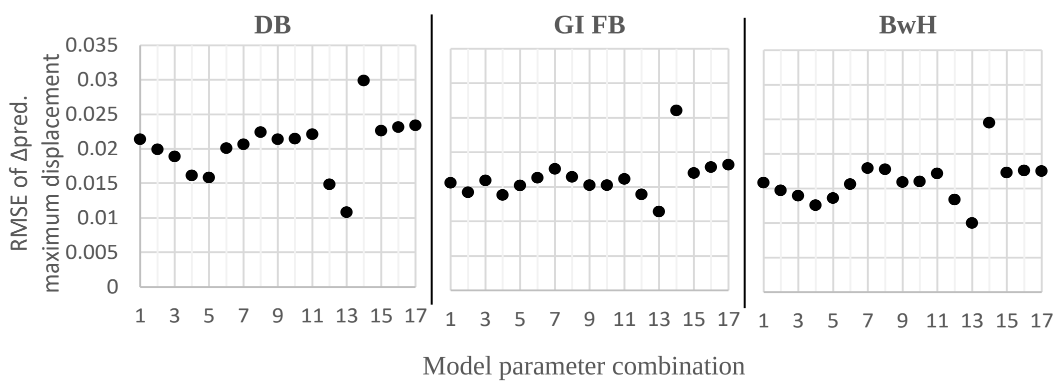

Figure 4. RMSE of predicted maximum drift ratio for all element formulations and model parameter combinations.

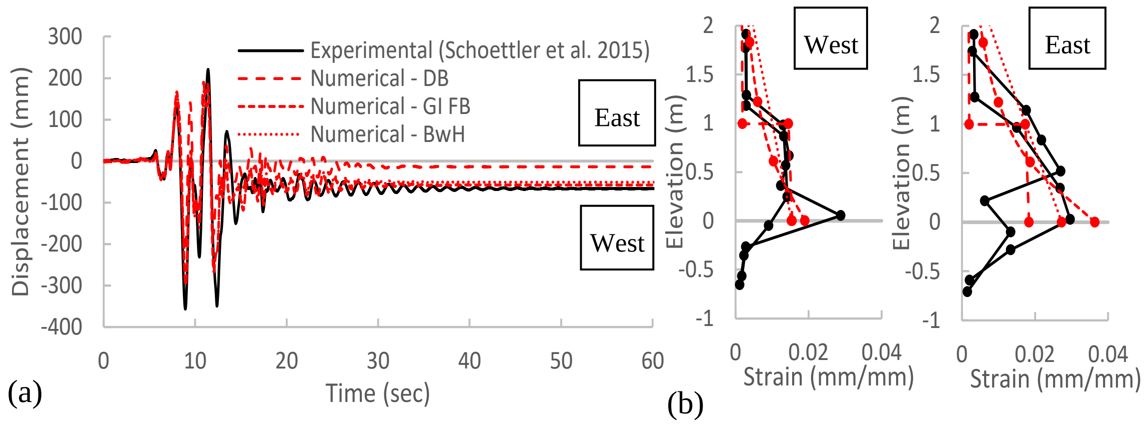

Figure 5. Experimentally measured versus numerically predicted (Comb. 1): (a) displacement time history of the top of the column, and (b) strain profile at maximum displacement for the PEER specimen under EQ3.

RESIDUAL DISPLACEMENT

μ and COV of the ratio of the predicted residual displacement ($\Delta^{\text{pred.}}_{\text{resid.}}$) to the measured residual displacement ($\Delta^{\text{meas.}}_{\text{resid.}}$), as well as RMSE of the predicted residual drift ratios for all element formulations and model parameter combinations, are presented in Table 4. Figs 6 and 7 plot μ and COV of $\Delta^{\text{pred.}}_{\text{resid.}}/\Delta^{\text{meas.}}_{\text{resid.}}$ for all element formulations and model parameter combinations, respectively. Fig. 8 plots the RMSE of the predicted residual drift ratios for all element formulations and model parameter combinations. Under-prediction was more pronounced for the residual displacement than the maximum displacement. This is evident by the lower means of the predicted-to-measured ratio of residual displacement than their maximum displacement counterparts, as seen in Tables 3 and 4. In addition, significantly higher dispersion was observed for residual displacements when compared to the maximum displacement. The COVs of $\Delta^{\text{pred.}}_{\text{resid.}}/\Delta^{\text{meas.}}_{\text{resid.}}$ ranged from 0.76 to 1.18, whereas those of $\Delta^{\text{pred.}}_{\text{max.}}/\Delta^{\text{meas.}}_{\text{max.}}$ ranged from 0.19 to 0.31. Residual displacements were also predicted with much less accuracy than the maximum displacement. While the RMSEs of the predicted maximum and residual drift ratios seem comparable, differences in accuracy are substantial. Note that the residual drift ratios are typically on the order of 10-20% of the maximum drift ratios. This makes, an RSME of 0.015, for example, unreasonably high for the predicted residual drift ratios though can be considered satisfactory for the predicted maximum drift ratios. Slight variation in COV of $\Delta^{\text{pred.}}_{\text{resid.}}/\Delta^{\text{meas.}}_{\text{resid.}}$ was observed across the three element formulations, as is apparent from Table 4. In terms of accuracy, none of the three element formulations demonstrated consistent superiority; the accuracy of the element formulations depended on the model parameter combination.

Switching from *Concrete04* to *Concrete01* had little impact on the predicted residual displacement, as evident by the comparable μ and COV of $\Delta^{\text{pred.}}_{\text{resid.}}/\Delta^{\text{meas.}}_{\text{resid.}}$ and RMSE of the predicted drift ratio for the three element formulations (Table 4). Predicted residual displacements were also sensitive to the change in reinforcing steel models, particularly *ReinforcingSteel* and *Dodd-Restrepo*. The two models resulted in higher predictions of residual displacement when compared to *Steel02*. Their effect on the accuracy of residual displacement predictions varied with the element formulation. Variation in bond slip models had limited influence on the μ and COV of $\Delta^{\text{pred.}}_{\text{resid.}}/\Delta^{\text{meas.}}_{\text{resid.}}$ as well as the RMSE of the predicted residual drift ratios. This indicates that reducing pinching in the hysteretic response by increasing R_c in *Bond SP01* is not an effective strategy to improve the accuracy of residual displacement predictions. Variation in μ and COV of $\Delta^{\text{pred.}}_{\text{resid.}}/\Delta^{\text{meas.}}_{\text{resid.}}$ as well as the RMSE of the predicted residual drift ratios in response to the change in the damping model were consistent with those observed for the maximum displacement. The only noticeable difference is that the extent to which the accuracy is improved when tangent stiffness is used is noticeably lower for the predicted residual drifts. Similar to maximum displacement, the accuracy of the predicted residual displacements was not improved when accounting for the strain rate effect. This is evident by the comparable RMSEs of Combs. 14-16 to that of Comb. 1 (see Table 4).

Table 4. Mean (μ) and coefficient of variation (COV) of ratio of predicted ($\Delta_{pred.}$) to measured ($\Delta_{meas.}$) residual displacement; and root-mean-square error (RMSE) of predicted residual drift ratio for all element formulations and model parameter combinations.

Comb.	Element formulation								
	DB			GI FB			BwH		
	μ	COV	RMSE	μ	COV	RMSE	μ	COV	RMSE
1	0.29	0.81	0.018	0.38	0.80	0.014	0.40	0.80	0.017
2	0.31	0.83	0.018	0.36	0.80	0.016	0.44	0.83	0.016
3	0.32	1.12	0.017	0.38	1.01	0.013	0.39	1.18	0.016
4	0.66	0.93	0.015	0.73	0.89	0.014	0.88	0.96	0.015
5	0.61	0.90	0.011	0.98	0.86	0.017	1.16	0.91	0.016
6	0.44	0.76	0.013	0.70	0.95	0.016	0.90	0.91	0.022
7	0.48	0.85	0.014	0.79	1.10	0.010	0.79	0.88	0.020
8	0.34	0.87	0.017	0.38	0.83	0.015	0.42	0.90	0.018
9	0.28	0.84	0.018	0.37	0.84	0.014	0.39	0.79	0.018
10	0.27	0.85	0.019	0.36	0.86	0.014	0.39	0.79	0.018
11	0.32	0.84	0.018	0.37	0.83	0.014	0.37	0.79	0.018
12	0.37	0.79	0.015	0.36	0.87	0.014	0.46	0.88	0.015
13	0.44	0.85	0.012	0.50	0.87	0.014	0.57	0.95	0.013
14	0.23	0.86	0.020	0.29	0.81	0.019	0.27	0.93	0.015
15	0.28	0.80	0.018	0.33	0.82	0.014	0.39	0.80	0.017
16	0.29	0.84	0.018	0.32	0.87	0.015	0.40	0.86	0.015
17	0.28	0.87	0.018	0.33	0.89	0.015	0.40	0.96	0.014

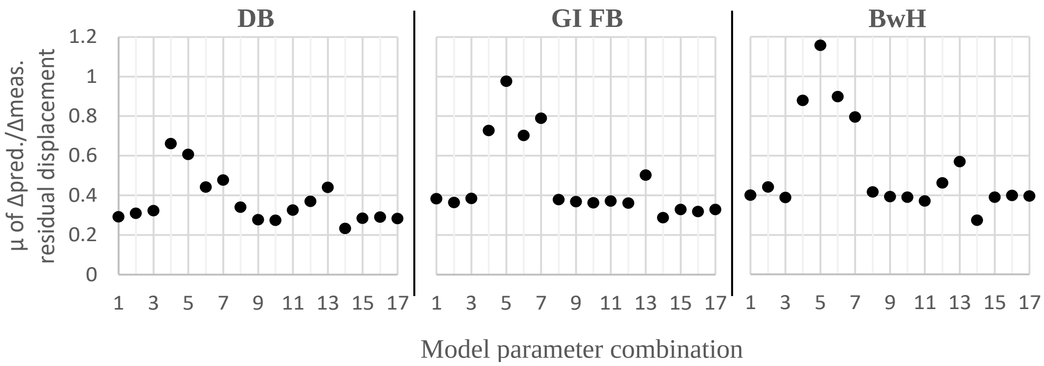

Figure 6. Mean (μ) of ratio of predicted to measured residual displacement for all element formulations and model parameter combinations.

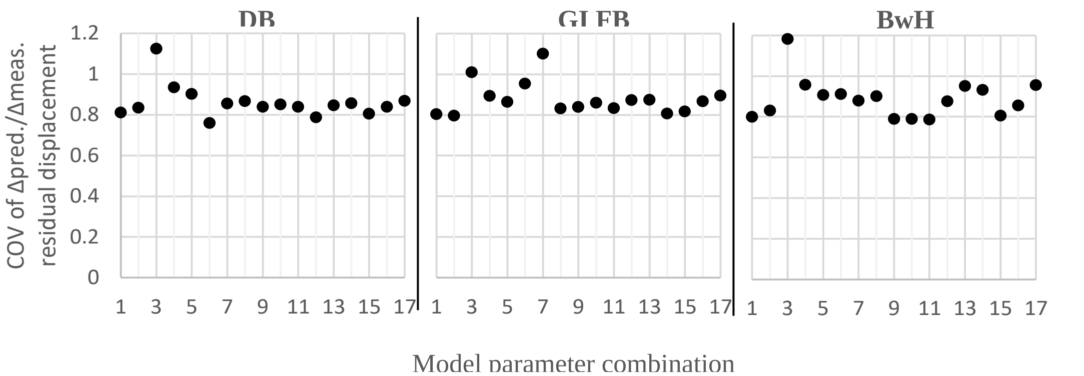

Figure 7. Coefficient of variation (COV) of ratio of predicted to measured residual displacement for all element formulations and model parameter combinations.

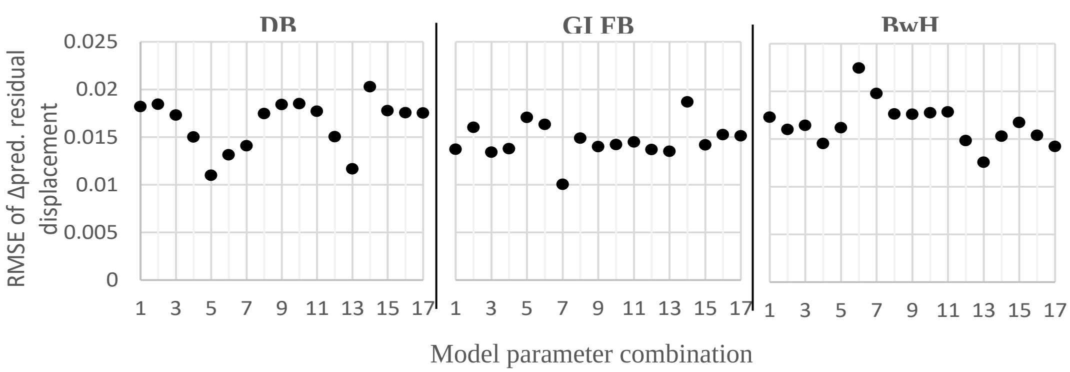

Figure 8. RMSE of predicted residual drift ratio for all element formulations and model parameter combinations.

CORRECTION FACTOR FOR RESIDUAL DISPLACEMENT PREDICATION

The previous observations showed that, unlike maximum displacement, residual displacements were predicted with unreasonably high levels of error, irrespective of the model parameter combination and element formulation. This indicates that, unless corrected, residual displacement is not suitable to be used as an engineering demand parameter within the context of PBSD. To improve the accuracy of residual displacement predictions, a correction factor is proposed herein. The previous results were reexamined to identify the model parameter combination and element type with the highest potential. Model parameter combinations and element formulations were first evaluated based on the accuracy of the predicted maximum displacement. This is because of the correlation between the predicted maximum and residual displacements [13]. In terms of maximum displacement, Comb. 13, yielded the most accurate predictions with RMSE of the predicted maximum drift ratio of 0.01 for the three element formulations. To select a single element formulation, RMSEs of the predicted residual drift ratio for the three element formulations for Comb. 13 were compared (see Table 4). DB element was characterized with the least RMSE of the predicted residual drift ratio. Data from Comb. 13 and DB element were thus used to develop the residual displacement prediction correction model. The data were fitted to mathematical expressions using an unconventional yet powerful type of regression, the symbolic regression. Unlike traditional regression where the model structure is fixed or user-specified, in symbolic regression, no particular model is provided as a starting point to the regression analysis. To discover the model structure and its parameters that best fit a given data set, symbolic regression typically uses genetic programming. This process starts with an initial set of random programs (often referred to as the “first generation”) which are continuously altered through selection, cross-over, and mutation rules in successive generations to produce new more accurate programs. The training set is used to generate and optimize programs, and the validation set is used to test the accuracy of those programs. The resulting correction factor (CF) from the symbolic regression takes the following form:

$$CF = 1.807\mathrm{PGA}^2 + (\mathrm{PGA} + T)^{-3.931} + \mathrm{PGA}^{-4.283}\left(0.0000177^{\left(\mathrm{PGV}\,T^2 + \mathrm{PGA}^{\left(2.340\,\mathrm{PGA}\,\mathrm{PGV}^{-6.346}\right)}\right)}\right) \quad (1)$$

Where PGA is the peak ground acceleration, expressed as a ratio to g, PGV is the peak ground velocity in m/sec, and T is the fundamental period of vibration of the column in seconds. Multiplying the predicted residual drift ratios for Comb. 13 reduced their RMSE to 0.0064 which is 45% less than that of the initial predictions. A scatter plot of the measured residual drift ratio ($\mathrm{RDR}_{\mathrm{meas.}}$) versus the predicted residual drift ratio ($\mathrm{RDR}_{\mathrm{pred.}}$) following correction is given in Fig. 9. The slope of the fitted line is a measure of the bias in the predictions. The closer the slope is to a value of 1, the less bias the prediction has in simulating the experimental results. Little bias in the predictions following correction can be observed, rendering the proposed correction factor effective and reliable.

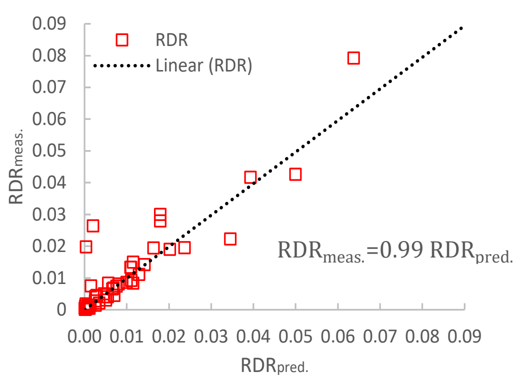

Figure 9. Scatter plot of experimentally measured residual drift ratio versus predicted residual drift ratio following correction with the proposed model (Eq. 1).

CONCLUSIONS

Accurate prediction of structural responses under earthquake excitations is fundamental to performance-based seismic design. The overarching objective of this study was to evaluate the accuracy and uncertainty of the predicted maximum and residual displacements by nonlinear time-history analysis. To achieve this objective, an analysis matrix considering a wide range of element formulation and model parameter combinations was first formulated. A series of nonlinear time-history analyses were performed to predict the maximum and residual displacements of reinforced concrete bridge columns previously tested under shake table excitations. The following conclusions were reached:

1. For a certain model parameter combination, variation in element formulation had little influence on the accuracy and uncertainty of the predicted maximum displacements. The gradient inelastic force-based element, however, predicted bar tensile strain profiles across the plastic hinge with higher resolution, but at a higher computational cost.
2. Models with tangent stiffness-based Rayleigh damping produced the most accurate predictions of maximum drift ratios with an RMSE of 0.011, indicating that the maximum displacement (or drift ratio) can be predicted with reasonable accuracy with the right model parameter combination.
3. Predictions of residual displacements were characterized by noticeably higher error and uncertainty when compared to predicted maximum displacement, irrespective of the element formulation and model parameter combination. This rendered predicted residual displacements unusable unless corrected.

A data-driven model was proposed to correct the predicted residual displacement. Following correction, the RMSE of the predicted residual drift ratio was reduced by 43% to 0.006.

ACKNOWLEDGEMENTS

The financial contributions of the Green Construction Research & Training Center (GCRTC) at the University of British Columbia (UBC) and the Natural Sciences and Engineering Research Council of Canada (NSERC) were critical to conduct this research.

REFERENCES

[1] Scott, M. H., and Fenves, G. L. 2006. "Plastic hinge integration methods for force-based Beam–Column elements." *Journal of Structural Engineering*, 132(2), 244-252.

[2] Calabrese, A., Almeida, J. P., and Pinho, R. 2010. "Numerical issues in distributed inelasticity modeling of RC frame elements for seismic analysis." *Journal of Earthquake Engineering*, 14(S1), 38-68.

[3] Feng, Y., Kowalsky, M. J., and Nau, J. M. 2014. "Fiber-based modeling of circular reinforced concrete bridge columns." *Journal of Earthquake Engineering*, 18(5), 714-734.

[4] Kashani, M. M., Lowes, L. N., Crewe, A. J., and Alexander, N. A. 2016. "Nonlinear fibre element modelling of RC bridge piers considering inelastic buckling of reinforcement." *Engineering Structures*, 116, 163-177.

[5] Salehi, M., Sideris, P., and Liel, A. B. 2020. "Assessing damage and collapse capacity of reinforced concrete structures using the gradient inelastic beam element formulation." *Engineering Structures*, 225, 111290.

[6] Pozo, J. D., Hube, M. A., and Yahya C. K. (2022). "Effective nonlinear simulations of RC columns with force-based elements." *Journal of Earthquake Engineering*, 1-22.

[7] Hachem, M. M., J. P. Moehle, and S. A. Mahin. 2003. *Performance of circular reinforced concrete bridge columns under bidirectional earthquake loading*. Rep. No. PEER-2003/06. Berkeley, CA: Pacific Earthquake Engineering Research Center, Univ. of California Berkeley.

[8] Sakai, J., S. A. Mahin, and A. Espinoza. 2006. *Earthquake simulation tests on reducing residual displacements of reinforced concrete bridge columns*. Rep. No. PEER-2005/17. Berkeley, CA: Pacific Earthquake Engineering Research Center, Univ. of California Berkeley.

[9] Berry, M. P., and Eberhard, M. O. 2008. Performance modeling strategies for modern reinforced concrete bridge columns. Rep. No. PEER-2007/07. Berkeley, CA: Pacific Earthquake Engineering Research Center, Univ. of California Berkeley.

[10] Stanton, J. F., and H. D. McNiven. 1979. *The development of a mathematical model to predict the flexural response of reinforced concrete beams to cyclic loads, using system identification*. Rep. No. UCB/EERC-79/02. Berkeley, CA: University of California, Berkeley, Earthquake Engineering Research Center.

[11] Lee, W. K., and S. L. Billington. 2010. "Modeling residual displacements of concrete bridge columns under earthquake loads using fiber elements." *J. Bridge Eng.*, 15 (3): 240–249.

[12] Moshref, A., M. Tehranizadeh, and M. Khanmohammadi. 2015. "Investigation of the reliability of nonlinear modeling approaches to capture the residual displacements of RC columns under seismic loading." *Bull. Earthquake Eng.*, 13 (8): 2327–2345.

[13] Yazgan, U., and A. Dazio. 2011a. "Simulating maximum and residual displacements of RC structures: I. Accuracy." *Earthquake Spectra*, 27 (4): 1187–1202.

[14] Yazgan, U., and A. Dazio. 2011b. "Simulating maximum and residual displacements of RC structures: II. Sensitivity." *Earthquake Spectra*, 27 (4): 1203–1218.

[15] Sousa, R., Almeida, J. P., Correia, A. A., and Pinho, R. 2020. "Shake table blind prediction tests: Contributions for improved fiber-based frame modelling." *Journal of Earthquake Engineering*, 24(9), 1435-1476.

[16] Akbari, S., and Khanmohammadi, M. 2021. "Prediction of residual and maximum displacement of concrete bridge columns under near-field motions using integrated experimental simulation data and distributed plasticity approaches." *Journal of Structural Engineering*, 147(12), 4021199.

[17] McKenna, F., G. L. Fenves, and M. H. Scott. 2000. *Open system for earthquake engineering simulation*. Berkeley, CA: University of California, Berkeley.

[18] Aldabagh, S., and Alam, M. S. (2022). Drift ratio limit states for circular concrete columns reinforced with different types of high-strength steel reinforcing bars. *Journal of Bridge Engineering*, 27(4), 04022007.

[19] Aldabagh, S., Hossain, F., and Alam, M. S. (2022). Simplified predictive expressions of drift limit states for reinforced concrete circular bridge columns. *Journal of Structural Engineering*, 148(3), 04021285.

[20] Sideris P., and Salehi M. 2016. "A gradient-inelastic flexibility-based frame element formulation." *J. Eng. Mech.*, 2016, 142(7), 04016039.

[21] Karsan, I. D., and Jirsa, J. O. 1969. "Behavior of concrete under compressive loadings." *J. Struct. Div.*, 95(12), 2543–2563.

[22] Scott, B., Park, R., and Priestley, M. N. 1982. "Stress-strain behavior of concrete confined by overlapping hoops at low and high strain rates." *J. Am. Concr. Inst.*, 79(1), 13–27.

[23] Popovics, S. (1973). "A numerical approach to the complete stress strain curve for concrete." *Cement and Concrete Research*, 3(5), 583-599.

[24] Stanton, J., and McNiven, H. 1979. *The development of a mathematical model to predict the flexural response of reinforced concrete beams to cyclic loads, using system identification*. Rep. No. EERC 79-02. Earthquake Engineering Research Center, Univ. of California, Berkeley, Calif.

[25] Mander J.B., Priestley M.J.N., and Park R. (1988). "Theoretical Stress-Strain Model for Confined Concrete." *Journal of Structural Engineering*, 114(8), 1804-1826.

[26] Menegotto, M., and P. Pinto. 1973. "Method of analysis for cyclically loaded reinforced concrete plane frames including changes in geometry and non-elastic behavior of elements under combined normal force and bending." In Vol. 11 *Proc., IABSE Symp. on Resistance and Ultimate Deformability of Structures Acted on by Well Defined Repeated Loads* 15–22. Zürich, Switzerland: International Association for Bridge and Structural Engineering.

[27] Dodd, L. L., and Restrepo-Posada, J. I. "Model for predicting cyclic behavior of reinforcing steel." *Journal of Structural Engineering*, 121(3), 433-445.

[28] Kunnath, S. K., Heo, Y., and Mohle, J. F. (2009). "Nonlinear uniaxial material model for reinforcing steel bars." *Journal of Structural Engineering*, 135(4), 335-343.

[29] Chang, G., and Mander, J. 1994. *Seismic energy based fatigue damage analysis of bridge columns: Part I—Evaluation of seismic capacity*. NCEER Technical Rep. No. 94-0006. Buffalo, N.Y.

[30] Zhao, J., and S. Sritharan. (2007). "Modeling of strain penetration effects in fiber-based analysis of reinforced concrete structures." *ACI Structural Journal*, 104(2), 133-141.

[31] Hall, J. F. 2006. "Problems encountered from the use (or misuse) of Rayleigh damping." *Earthquake Eng. Struct. Dyn.*, 35 (5): 525–545.

[32] Charney, F. A. 2008. "Unintended consequences of modeling damping in structures." *J. Struct. Eng.*, 134 (4): 581–592.

[33] Chopra, A. K., and F. McKenna. 2016. "Modeling viscous damping in nonlinear response history analysis of buildings for earthquake excitation." *Earthquake Eng. Struct. Dyn.*, 45 (2): 193–211.

[34] Jeong, H. I., J. Sakai, and S. A. Mahin. 2008. *Shaking table tests and numerical investigation of self-centering reinforced concrete bridge columns*. Rep. No. PEER-2008/06. Berkeley, CA: Pacific Earthquake Engineering Research Center.

[35] Petrini, L., Maggi, C., Priestley, M. J. N., and Calvi, G. M. 2008. "Experimental verification of viscous damping modeling for inelastic time history analyzes." *Journal of Earthquake Engineering*: JEE, 12(sup1), 125-145.

[36] Malvar, L.J. 1998. "Review of static and dynamic properties of steel reinforcing bars." *ACI Materials Journal*, 95(5), 609–616.

[37] Paulay, T., and Priestley, M. J. N. 1992. *Seismic design of reinforced concrete and masonry buildings*. Wiley, New York.

[38] Laplace, P. N., Sanders, D, Saiidi, M. S., and Douglas, B. 1999. *Shake table testing of flexure dominated reinforced concrete bridge columns*. Report No. CCEER 99-13. Reno, NV: Univ. of Nevada, Reno, Center for Earthquake Engineering Research.

[39] Phan, V. T. 2005. "Near fault (near field) ground motion effects on reinforced concrete bridge columns." M.Sc. Thesis, University of Nevada, Reno.

[40] Choi, H. 2007. "Effects of near-fault ground motion and fault-rupture on the seismic response of reinforced concrete bridges." Ph.D. Dissertation, University of Nevada, Reno.

[41] Schoettler, M. J., J. I. Restrepo, G. Guerrini, D. E. Duck, and F. Carrea. 2015. *A full-scale, single-column bridge bent tested by shake-table excitation*. PEER Rep. No. 2015/02. Berkeley, CA: Pacific Earthquake Engineering Research Center (PEER), Univ. of California.

[42] Mohammed, M. S. 2016. "Effect of earthquake duration on reinforced concrete bridge columns." Ph.D. Dissertation, University of Nevada, Reno.